Theory for the electromigration wind force in dilute alloys

J. P. Dekker and A. Lodder
Faculteit Natuurkunde en Sterrenkunde, Vrije Universiteit, De Boelelaan 1081, 1081 HV Amsterdam, The Netherlands

J. van Ek
Department of Physics, Tulane University, New Orleans, Louisiana 70118
(Received 15 April 1997)

A multiple scattering formulation for the electromigration wind force on atoms in dilute alloys is developed. The theory describes electromigration via a vacancy mechanism. The method is used to calculate the wind valence for electromigration in various host metals having a close-packed lattice structure, namely aluminum, the noble metals copper, silver, and gold, and the 4*d* transition metals. The self-electromigration results for aluminum and the noble metals compare well with experimental data. For the 4*d* metals small wind valences are found, which make these metals attractive candidates for the experimental study of the direct valence. [S0163-1829(97)00643-7]

I. INTRODUCTION

An electric field, applied to a metal sample, causes an atomic current, besides the common electric current. This process is called electromigration and has been studied for many years. Coehn and Specht[1] reported a flow of hydrogen atoms towards the cathode in palladium. This migration of interstitial atoms is a rather harmless manifestation of the effect. It offers the possibility to influence the concentration profile of impurity atoms along a sample. However, a net flow of host atoms can also be the consequence of applying an electric field. Clearly, this reduces the conductivity of a metal wire because of the formation of voids on one side and hillocks on the other side. In wires of normal size this turns out not to be of great importance, because the atoms do not move very fast. In thin films, however, the situation is different. Thin films can carry higher current densities, because the heat, produced by the current, is transfered more easily to the environment. Therefore they can endure a current density greater than 10^7A/cm^2, while a bulk sample would melt when the current density is 10^4A/cm^2. Electromigration damage in aluminum films is a well-known example.

The migration of atoms turns out to be influenced by the presence of impurities. Most important is the effect of copper doping of Al films, which greatly reduces the electromigration damage. This effect has been known for a long time but without an understanding of it, so impurities have been added using the method of trial and error. Furthermore, although the damage appears too fast for a device user, it is still not fast enough for an experimental physicist. So, the effect is studied under so-called accelerated conditions, i.e., high temperatures and high current densities. Unfortunately, the extrapolation to user conditions is not trivial, because the total atomic flow is a result of a number of competing contributions with different activation energies. All of this complicates the picture and demands a theoretical framework, to which this paper is aimed to contribute.

Two ingredients are essential in the process of electromigration, namely diffusion and a driving force. The motion of atoms due to diffusion is random. At lower temperatures diffusion along grain boundaries is dominant, but at high temperatures bulk diffusion becomes the most important contribution. For accelerated conditions it is the leading mechanism and the atoms move by exchanging positions with vacancies. The second ingredient, the driving force, introduces a bias into the random motion of atoms. One contribution to that force is calculated in the present work, namely the wind force due to scattering of electrons by the moving atom, which can be either a host atom or an impurity atom. A well-established quantum-mechanical expression for the wind force is available.[2] Besides the wind force, the driving force has a direct part. If the nuclear charge is not completely screened, the electric field directly pushes the atom towards the cathode. This force has been the subject of a controversy for many years.[3,4] Both contributions are proportional to the electric field and the total driving force can therefore be written as

$$\mathbf{F}=\mathbf{F}_{\text{wind}}+\mathbf{F}_{\text{direct}}=(Z_{\text{wind}}+Z_{\text{direct}})e\mathbf{E}=Z^{*}e\mathbf{E}. \qquad (1)$$

The effective valence Z^*, which is the sum of the wind and direct valence, has been measured for a lot of systems.[3] Often the wind force dominates the direct force and, depending on the system, the resulting total force can push the atom either to the anode or to the cathode.

The calculation of the wind force requires knowledge of the electronic structure of the alloy. An impurity in a dilute alloy, in which the concentration of impurities is low, only interacts with its direct environment of host atoms. The electrons feel a potential, which only differs from the host potential in a small cluster of atoms containing the migrating atom, the vacancy, and the surrounding host atoms affected by charge transfer and lattice deformation. A Green's function formulation of multiple scattering theory is used to calculate the electron wave function in the dilute alloy. This formalism is an extension of the Korringa-Kohn-Rostoker (KKR) method for the calculation of the band structure of a metal.[5,6] The alloy is described with respect to a reference system. The conventional choice of this reference system is the host metal, but then the electronic structure of the impor-

tant saddle point configuration in electromigration cannot be described. This is due to the fact that the atoms in the alloy system cannot be mapped onto the ones in the host system one-to-one. As proposed by Lodder[7] an intermediate void system is used, which does not contain any scatterers in the perturbed region. The original formulation,[8] in which the cluster of perturbed atoms is considered as a whole, was recently applied in a preliminary study of electromigration in copper and aluminum.[9] This formulation is rather cumbersome and in the mean time we found a simpler single site formulation, in which each atom in the cluster is considered separately, analogous to the formalism used for the description of interstitial impurities by Oppeneer and Lodder[10] and van Ek.[11] The validity of this method is not limited to the particular problem of substitutional electromigration. In all problems concerning dilute alloys the wave function can be calculated this way.

The multiple scattering expression for the wind force is elaborated in Sec. II. This section contains two subsections, devoted to the wave function and the Green's function matrix, respectively. In Sec. III some details of the calculation are given. The formalism is applied to metals with a close-packed lattice structure in Sec. IV. Self-electromigration and impurity electromigration in Al are treated in Sec. IV A, self-electromigration in the noble metals as well as impurity migration in Ag in Sec. IV B, and self-electromigration in $4d$ transition metals in Sec. IV C. In Sec. V the main results of this paper are summarized.

Throughout the paper atomic units are used, such that $\hbar=2m=1$. Exceptions are stated explicitly.

II. MULTIPLE-SCATTERING EXPRESSION FOR THE WIND FORCE

In this section the quantum-mechanical equation for the wind force of Sorbello *et al.*[2]

$$\mathbf{F}_{\text{wind}}=\sum_k \delta f(k)\langle\Psi_k|-\nabla_{\mathbf{R}_p}v_p|\Psi_k\rangle, \tag{2}$$

which traces back to the pioneering work of Bosvieux and Friedel,[12] and in which

$$\delta f(k)=e\tau_k\mathbf{E}\cdot\mathbf{v}_k df_0(\epsilon_k)/d\epsilon_k, \tag{3}$$

is expressed in computable quantities. In Eq. (2) the alloy electron wave function, Ψ_k, is supposed to be constructed from the corresponding Bloch function, labeled by crystal momentum $\mathbf{k}$ and band index n, combined in $k=(\mathbf{k},n)$, and having an energy eigenvalue ϵ_k. In a simple ballistic picture momentum is transfered from electrons to the atom because of scattering, resulting in the wind force. The momentum transfered to this atom, with a potential v_p centered at position $\mathbf{R}_p$ in the alloy, is proportional to the expectation value of the force operator $-\nabla_{\mathbf{R}_p}v_p$. When no electric field is present, the electrons are distributed according to the Fermi-Dirac function $f_0(\epsilon_k)$, leading to an exact cancellation of forces. In other words, each push from the electrons in one direction is compensated, on the average, by one in the opposite direction. This symmetry is broken by the presence of the electric field, which alters the distribution function by $\delta f(k)$. The first and leading term of this deviation, Eq. (3), is linear in the applied electric field $\mathbf{E}$ and proportional to the electron transport relaxation time τ_k. In Eq. (3) e is the elementary charge and $\mathbf{v}_k$ is the velocity of the electron. As usual, in all applications, the transport relaxation time is taken constant throughout the Brillouin zone. All other quantities can be extracted from the electronic structure. The method for the calculation of the electron wave function originally provided by Lodder[8] will be used in a modified way.

In the present formulation the crystal is divided into cells. For the host crystal these cells are the well-known Wigner-Seitz cells containing local potentials $v^h(\mathbf{x})$. For the alloy these cells may have a different shape in the region of the impurity cluster and they contain local potentials $v^p(\mathbf{x})$. The local potentials v^h and v^p consist of a spherical atomic potential surrounded by an interstitial region, where the potential is constant. In order to evaluate the matrix element appearing in Eq. (2), the wave function is expanded in the pth cell, centered at $\mathbf{R}_p$. In such a cell the wave function $\Psi_k(\mathbf{r})=\Psi_k(\mathbf{x}+\mathbf{R}_p)$ can be written as a linear combination of regular solutions R_L^p of the Schrödinger equation with local potential v^p, so

$$\Psi_k(\mathbf{x}+\mathbf{R}_p)=\sum_L c_{kpL}R_L^p(\mathbf{x}), \tag{4}$$

where $L=(l,m)$ combines the angular momentum and magnetic quantum numbers. The expansion coefficients c_{kpL} will be derived in Sec. II A. The basis functions R_L^p are constructed such that outside the atomic sphere they have the free-space form

$$R_L^p(\mathbf{x})=j_L(\mathbf{x})-i\sum_{L'} t_{LL'}^p h_{L'}^+(\mathbf{x}), \tag{5}$$

where $j_L(\mathbf{x})$ is the product of a spherical Bessel function $j_l(\kappa x)$ and a spherical harmonic $Y_L(\hat{x})$, $h_L^+(\mathbf{x})$ is a similar product for the spherical Hankel function $h_l^+(\kappa x)$, $\kappa=\sqrt{E}$ and t^p is the scattering matrix for the potential v^p embedded in free space. For a spherically symmetrical scatterer this matrix is diagonal and equals $t_{LL'}^p=-\sin\eta_l^p e^{i\eta_l^p}\delta_{LL'}$, the η being the phase shifts.

In that case the wind force expression (2) can be elaborated to the form

$$\mathbf{F}_{\text{wind}}=\sum_k \delta f(k)2\ \text{Re}\sum_L \sum_{m_1=-(l+1)}^{l+1} c_{kpL}^*\mathbf{D}_{L;l+1,m_1} \times\sin(\eta_{l+1}-\eta_l)e^{i(\eta_{l+1}-\eta_l)}c_{kpl+1,m_1}, \tag{6}$$

according to Eqs. (26) and (31) in Ref. 8, in which the vectorial matrix $\mathbf{D}$ is defined as

$$\mathbf{D}_{LL'}=\int d\hat{x}Y_L(\hat{x})\hat{x}Y_{L'}(\hat{x}). \tag{7}$$

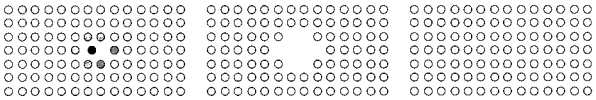

FIG. 1. The systems used in the description of the dilute alloy (left): the void system (center) and the host system (right).

A. The wave function coefficients

The alloy wave function coefficients that appear in Eq. (4) will be expressed in terms of wave function coefficients c^{host}_{kjL}, which appear in the local expansion of Bloch function $\Psi^{\mathrm{host}}_k(\mathbf{r})=\Psi^{\mathrm{host}}_k(\mathbf{x}+\mathbf{R}_j)$,

$$\Psi^{\mathrm{host}}_k(\mathbf{x}+\mathbf{R}_j)=\sum_L c^{\mathrm{host}}_{kjL}R^j_L(\mathbf{x}), \tag{8}$$

where R^j_L are the regular solutions of the Schrödinger equation within the Wigner-Seitz cell labeled by j and contain t^h instead of t^p in their asymptotic form [see Eq. (5)]. Unperturbed atomic positions $\mathbf{R}_j$ in the host do not necessarily coincide with one of the atomic positions $\mathbf{R}_p$ in the alloy. The number of alloy sites may even differ from the number of host lattice sites. Therefore, although the alloy is described with respect to the host, the host system cannot be used as a reference system straightforwardly. An intermediate system is required, which will be referred to as the void system. This system consists of a void region, where the potential is constant, surrounded by host atom potentials. The void region is chosen to be as extended as the perturbed region in the dilute alloy. This system can serve as a reference system for both the host and the alloy, as it is represented symbolically in Fig. 1. The relation between the host and alloy wave function is given via the void wave function. The alloy wave function is expressed in terms of the void wave function by the Green's function expression,[8]

$$\Psi_k=\Psi^{\mathrm{void}}_k+G^{\mathrm{void}}\sum_p v^p\Psi_k. \tag{9}$$

Analogously to Eqs. (4) and (8) the void wave function can be written in terms of local basis functions, being spherical Bessel functions because of the constant potential in the void region

$$\Psi^{\mathrm{void}}_k(\mathbf{x}+\mathbf{R}_p)=\sum_L c^{\mathrm{void}}_{kpL}j_L(\mathbf{x}). \tag{10}$$

Inside the void, the void Green's function can be written as

$$G^{\mathrm{void}}(\mathbf{x}+\mathbf{R}_p,\mathbf{x}'+\mathbf{R}_{p'})=-i\kappa\sum_L j_L(\mathbf{x}_<)h^+_L(\mathbf{x}_>)\delta_{pp'}+\sum_{LL'} j_L(\mathbf{x})\mathcal{G}^{\mathrm{void},pp'}_{LL'}j_{L'}(\mathbf{x}'). \tag{11}$$

This expression with the void Green's function matrix $\mathcal{G}^{\mathrm{void},pp'}$ is a straightforward generalization of the expression for the Green's function of free space

$$G^0(\mathbf{x}+\mathbf{R}_p,\mathbf{x}'+\mathbf{R}_{p'})=-i\kappa\sum_L j_L(\mathbf{x}_<)h^+_L(\mathbf{x}_>)\delta_{pp'}\times\sum_{LL'} j_L(\mathbf{x})B^{pp'}_{LL'}j_{L'}(\mathbf{x}'), \tag{12}$$

in which the free-space propagation matrix B appears, defined as

$$B^{pp'}_{LL'}\equiv B_{LL'}(\mathbf{R}_{pp'})=4\pi i^{l-l'-1}\kappa(1-\delta_{pp'})\sum_{L''} i^{l''}C_{LL'L''}h^+_{L''}(\mathbf{R}_{pp'}). \tag{13}$$

The void Green's function matrix will be given in Sec. II B.

Combining Eqs. (9), (10), and (11) the following matrix equation can be found:

$$c^{\mathrm{void}}_{kpL}=\sum_{p'L'}(1-\mathcal{G}^{\mathrm{void}}t)^{pp'}_{LL'}c_{kp'L'}. \tag{14}$$

Details of the derivation will be given in Appendix A. Following the same procedure, void wave function coefficients carrying the host position label j can be expressed in terms of host coefficients c^{host}_{kjL},

$$c^{\mathrm{void}}_{kjL}=\sum_{j'L'}(1-\mathcal{G}^{\mathrm{void}}t^h)^{jj'}_{LL'}c^{\mathrm{host}}_{kj'L'}. \tag{15}$$

Since c^{void}_{kpL} and c^{void}_{kjL} are related by

$$c^{\mathrm{void}}_{kpL}=\sum_{L_1} J^{pj}_{LL_1}c^{\mathrm{void}}_{kjL_1}, \tag{16}$$

Eqs. (14) and (15) can be combined to

$$\sum_{p'L'}(1-\mathcal{G}^{\mathrm{void}}t)^{pp'}_{LL'}c_{kp'L'}=\sum_{j'L'L_1}J^{pj}_{LL_1}(1-\mathcal{G}^{\mathrm{void}}t^h)^{jj'}_{L_1L'}c^{\mathrm{host}}_{kj'L'}. \tag{17}$$

It is noteworthy that in this equation two types of summations over the angular momentum occur. The first type has a natural cutoff because of the multiplication by t matrices, and the second type, such as the summation over L_1, in principle runs to infinity. The latter summation can be treated analytically, to be shown in Appendix B, and the final equation used in the actual calculations,

$$\sum_{p'}(1-\mathcal{G}^{\mathrm{void}}t)^{pp'}c_{kp'}=b(\mathbf{k},\mathbf{R}_{pj})e^{i\mathbf{k}\cdot\mathbf{R}_{pJ}}t^hc^{\mathrm{host}}_{kj}-\sum_{j'}\mathcal{G}^{\mathrm{void},pj'}t^hc^{\mathrm{host}}_{kj'}, \tag{18}$$

only contains summations with a natural cutoff. Angular momentum labels have been dropped in order to simplify the notation. The matrix $b(\mathbf{k},\mathbf{R})$ is defined by

$$b(\mathbf{k},\mathbf{R})=\sum_{j'} B(\mathbf{R}-\mathbf{R}_{j'})e^{-i\mathbf{k}\cdot(\mathbf{R}-\mathbf{R}_{j'})}, \tag{19}$$

in which the summation runs over *all* lattice sites.

The host wave function coefficients occurring in Eq. (18) are calculated by the KKR method according to

$$\sum_{L'} M_{LL'}(\mathbf{k})t^h_{l'}c^{\text{host}}_{kjL}=0. \tag{20}$$

This equation contains the KKR matrix

$$M(\mathbf{k})=t^{h^{-1}}-b(\mathbf{k}), \tag{21}$$

in which $b(\mathbf{k})=b(\mathbf{k},0)$, defined by Eq. (19).

In its original form the KKR method applies to muffin-tin potentials. However, as shown by Nesbet,[13] it is possible to circumvent this restriction on the crystal potential in the same way as has been done in the derivation of Eq. (17). Now we will use this procedure in the calculation of the void Green's function.

B. The void Green's function

The void Green's function and the host Green's function G^h are related by the Lippmann-Schwinger equation,

$$G^{\text{void}}=G^h-G^h\sum_j v^h_j G^{\text{void}}. \tag{22}$$

The summation runs over the positions in the void. This equation is again evaluated in the position representation. The host Green's function is given by

$$G^h(\mathbf{x}+\mathbf{R}_j,\mathbf{x}'+\mathbf{R}_{j'})=\sum_L R_L(\mathbf{x}_<)S_L(\mathbf{x}_>)\,\delta_{jj'} + \sum_{LL'} R_L(\mathbf{x})\mathcal{G}^{jj'}_{LL'}R_L(\mathbf{x}'). \tag{23}$$

Outside the atomic sphere the regular solutions R_L of the local Schrödinger equation have the asymptotic form of Eq. (5) with t^p replaced by t^h and the singular solutions S_L equal $-i\kappa h^+_L$. First the void Green's function matrix $\mathcal{G}^{\text{void},jj'}$, carrying host position labels j and j', will be expressed in terms of the host Green's function matrix $\mathcal{G}^{jj'}$, to be determined later. To that end Eq. (22) is elaborated at the positions $\mathbf{x}+\mathbf{R}_j$ and $\mathbf{x}'+\mathbf{R}_{j'}$, where both $\mathbf{x}$ and $\mathbf{x}'$ are located close to their cell centers $\mathbf{R}_j$ and $\mathbf{R}_{j'}$ respectively. Following similar steps as in Appendix A one finds the relation

$$\mathcal{G}^{\text{void},jj'}=\mathcal{G}^{jj'}-\sum_{j_1}\mathcal{G}^{jj_1}t^h\mathcal{G}^{\text{void},j_1j'}, \tag{24}$$

where the angular momentum labels have been dropped. The matrix t^h is the same at all lattice sites, so the site label has been dropped. Iteration of this equation leads to

$$\mathcal{G}^{\text{void},jj'}=\mathcal{G}^{jj'}-\sum_{j_1j_2}\mathcal{G}^{jj_1}(t^{h^{-1}}+\mathcal{G})^{-1}_{j_1j_2}\mathcal{G}^{j_2j'}. \tag{25}$$

The host Green's function matrix $\mathcal{G}$ is calculated using the Lippmann-Schwinger equation,

$$G^h=G^0+G^0\sum_j v^h_j G^h, \tag{26}$$

G^0 being the free-space Green's function. The summation runs over all host lattice sites. Working in the position representation and using Eqs. (12) and (23) one finds the following matrix equation:

$$\mathcal{G}^{jj'}=B^{jj'}+\sum_{j_1}B^{jj_1}t^h\mathcal{G}^{j_1j'}. \tag{27}$$

Taking the Fourier transform of this equation one finds

$$\mathcal{G}(\mathbf{k})\equiv\sum_{j'}\mathcal{G}^{jj'}e^{i\mathbf{k}\cdot\mathbf{R}_{JJ'}}=b(\mathbf{k})+b(\mathbf{k})t^h\mathcal{G}(\mathbf{k}). \tag{28}$$

This equation can be solved for $\mathcal{G}(\mathbf{k})$,

$$\mathcal{G}(\mathbf{k})=[1-b(\mathbf{k})t^h]^{-1}b(\mathbf{k}) =b(\mathbf{k})+b(\mathbf{k})M^{-1}(\mathbf{k})b(\mathbf{k}), \tag{29}$$

containing the KKR matrix, Eq. (21). For the reverse Fourier transform, using the right hand side of this equation, one obtains

$$\mathcal{G}^{jj'}=\frac{1}{\Omega_{\text{BZ}}}\int_{\text{BZ}}d^3k[b(\mathbf{k})+b(\mathbf{k})M^{-1}(\mathbf{k})b(\mathbf{k})]e^{i\mathbf{k}\cdot\mathbf{R}_{JJ'}}, \tag{30}$$

in which the $\mathbf{k}$ summation has been replaced by an integral over the Brillouin zone (BZ) with volume Ω_{BZ}.

By now, expressions for $\mathcal{G}^{\text{void}}$ and $\mathcal{G}$ have been derived for centers j of host cells only. Interestingly, the generalized relation

$$\mathcal{G}^{\text{void},nn'}=\mathcal{G}^{nn'}-\sum_{j_1j_2}\mathcal{G}^{nj_1}(t^{h^{-1}}+\mathcal{G})^{-1}_{j_1j_2}\mathcal{G}^{j_2n'} \tag{31}$$

turns out to be valid also, carrying arbitrary position labels n and n', which can refer to host as well as alloy positions. The host Green's function matrix $\mathcal{G}^{nn'}$ is calculated from

$$\mathcal{G}^{nn'}\equiv\frac{1}{\Omega_{\text{BZ}}}\int_{\text{BZ}}d^3k[b(\mathbf{k},\mathbf{R}_{nn'}) +b(\mathbf{k},\mathbf{R}_n)M^{-1}(\mathbf{k})b^T(-\mathbf{k},\mathbf{R}_{n'})]e^{i\mathbf{k}\cdot\mathbf{R}_{nn'}}, \tag{32}$$

in which the matrix $b(\mathbf{k},\mathbf{R})$ is defined in Eq. (19). The derivation is given in Appendix B.

Equation (18), together with Eqs. (31) and (32), are the key equations of the theory presented. The alloy wave function coefficients c_{kpL} can be calculated, if the host wave function coefficients c^{host}_{kjL} and the matrix $\mathcal{G}^{\text{void}}$ are known. The host wave function coefficients can be calculated using the KKR equation (20). The matrix $\mathcal{G}^{\text{void}}$ can be calculated after evaluation of the Brillouin zone integral in Eq. (32).

III. COMPUTATIONAL DETAILS

In this section a few quantities which are necessary in the calculation are discussed. As mentioned in Sec. II the transport relaxation time τ is estimated from the measured resistivity. The procedure is given in Sec. III A. The construction

of the potentials is discussed in Sec. III B. Finally, the procedure for the extraction of measurable quantities from the calculations is explained in Sec. III C.

A. The transport relaxation time τ

Upon accepting the widely used isotropic transport relaxation time approximation for τ, the bulk conductivity (or the inverse bulk resistivity) for cubic crystals is given by[14]

$$\sigma=\frac{1}{\rho}=\frac{e^2\tau}{4\pi^3\hbar}\frac{1}{3}\int_{\mathrm{FS}}dS_k v_k . \tag{33}$$

The integral of the electron velocity v_k over the Fermi surface is directly computable from the electronic structure of the host metal. The only quantity left is the transport relaxation time τ, to which the wind force is directly proportional as can be seen from Eqs. (2) and (3). Combining Eqs. (1), (2), (3), and (33), the temperature dependent wind valence can be written as

$$Z_{\mathrm{wind}}(T)=\frac{K(T)}{\rho(T)}. \tag{34}$$

The temperature dependence of K comes from the temperature dependence of the Fermi-Dirac function appearing in Eq. (3) and can be neglected up to the melting temperature of most metals. The remaining temperature dependence of the wind valence through the resistivity is well known from the ballistic model by Fiks[15] and Huntington and Grone[16] and from later more sophisticated models.[17]

It should be noted that the calculated transport relaxation time can differ considerably from the free-electron transport Drude relaxation time, τ^{FE}, arising from the equation

$$\sigma=\frac{1}{\rho}=\frac{ne^2\tau^{\mathrm{FE}}}{m}. \tag{35}$$

τ can be as much as a factor of 17 larger than τ^{FE}, as was found for palladium.[18]

B. Potentials

Both the host and alloy potentials are modeled by muffin-tin potentials.[19] The corresponding phase shifts, *c.q.* the t matrices t^h and t^p, serve as input for the computational procedure. The alloy potentials are constructed only for two positions of the migrating atom: the initial position and the position half-way, the saddle point. When the atom is somewhere else along the path, which runs along a straight line in the $\langle 110\rangle$ direction, the phase shifts are calculated using the interpolation formula

$$\eta_l^p(s)=\cos^2(\pi s)\,\eta_l^p(0)+\sin^2(\pi s)\,\eta_l^p(\tfrac{1}{2}). \tag{36}$$

The variable s runs from 0 to 1 along the path, so $\eta_l^p(0)=\eta_l^{p,\mathrm{initial}}$ and halfway $\eta_l^p(\frac{1}{2})=\eta_l^{p,\mathrm{saddlepoint}}$, where p refers to one of the perturbed atoms in the cluster or to the migrating atom. The s dependence of the interpolation formula guarantees a smooth behavior of the phase shifts at the saddle point.

A parameter, which influences the results of the calculation, is the muffin-tin radius. The choice of this parameter is bound by two conflicting conditions. On the one hand it must be small enough to leave some room for the migrating atom, while on the other hand it must be large enough such that the potential still reproduces the electronic properties of the metal as much as possible. For fcc metals a muffin-tin radius of $0.325a$ is an optimal value.[20]

A real physical system is charge neutral. This can be established using a generalized Friedel sum rule[21] and a shifting procedure proposed by Lasseter and Soven[22] and successfully applied in numerous systems. The potential of the atom is shifted by a constant value, which can be interpreted as the addition of charge on the muffin-tin sphere. For the different configurations during the jump various choices are possible for the shift procedure. If the migrating atom is in its initial position, the simplest choice is a shift of the potentials of all nearest neighbors of the vacancy by the same value. In the saddle point configuration all nearest neighbors of the two small moon-shaped vacancies surrounding the migrating atom can be shifted. We want to point out that in the latter configuration the small vacancies are not accounted for, which means that the shifting procedure also must correct for the corresponding loss of charge in that region of space. This makes it unclear, what the shifting procedure means for the electronic properties. Due to these uncertainties and the lack of self-consistent potentials we therefore have decided to use the phase shifts corresponding to the unshifted potentials. Test calculations show that the potential shift leads to a maximum change in the wind valence of about 10% and in most cases of only a few percent. In view of the limited accuracy of most measurements this is acceptable for the time being. In principle full-potential calculations can reveal detailed information of the charge state of the impurity cluster.

C. Comparison with experiment

The calculated wind valence is a position dependent second-rank tensor. In order to compare with experiment the tensor has to be reduced to a scalar. The relevant component of the force is the one in the direction of the migration path, which we indicate by $\hat{s}$. Averaging over all orientations of the lattice, simulating the polycrystalline samples used in practice, we yield for the scalar wind valence

$$Z_{\mathrm{wind}}=\hat{s}^T\cdot\underline{Z_{\mathrm{wind}}}\cdot\hat{s}. \tag{37}$$

This scalar value must be averaged over the path, because the average force is the work done by it during the jump divided by the length of the path. By this a frequently used assumption, in which the wind force is taken as the average of its values at the initial and saddle point position,[23] can be tested.

IV. RESULTS FOR fcc METALS

The formalism described above is applied to metals with the close-packed face-centered cubic (fcc) and hexagonal close-packed (hcp) structures, the latter being replaced by its equivalent fcc structure. Wind valences are calculated for diffusing atoms in aluminum, the noble metals, and the $4d$ transition metals and are compared to experimental data and results from previously published computational studies.

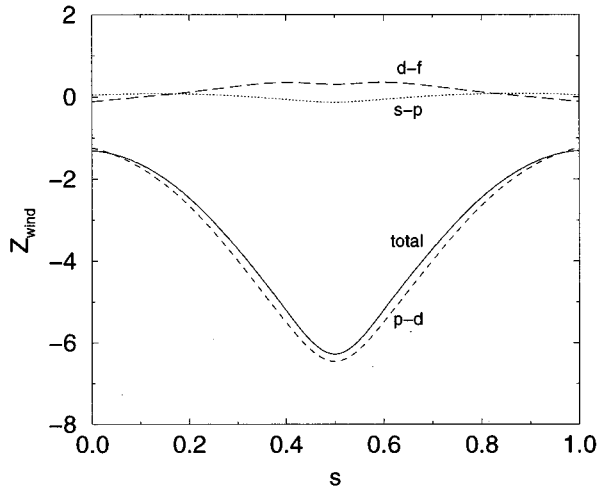

FIG. 2. The variation of the wind valence of a migrating host atom in aluminum at 800 K. The sp, pd, and df contributions are given separately.

A. Electromigration in aluminum

1. Self-electromigration

In Fig. 2 the solid line shows the variation of the scalar wind valence of a host atom in aluminum metal along the migration path. In addition the three partial wave contributions to Z_{wind} are shown, namely the sp, pd, and df contributions, depending on the differences $\eta_{l+1}-\eta_l$ as they appear in the expression for the matrix element $\langle\Psi_k|-\nabla_{\mathbf{R}_p}v_p|\Psi_k\rangle$ in Eq. (6). The pd term is dominant which is consistent with the values of the phase shifts of the moving aluminum atom, being 0.338, 0.395, 0.051, and 0.002 for s, p, d, and f, respectively, at the initial position and 0.370, 0.430, 0.056, and 0.002 at the saddle point. A sinusoidal behavior of the wind valence along the path would justify the averaging procedure, which uses the values in initial and saddle point position only. Such a behavior seems to be obeyed in the figure. In Table I results for the initial and saddle point position, their average value and the average over the path are listed. In the first three columns the three partial contributions are shown. The fourth contains the sum of the three. In order to obtain these values the transport relaxation time of $\tau=69$ a.u. has been calculated using Eq. (33), assuming the resistivity to equal the phonon part at 800 K, namely $\rho=8.6\ \mu\Omega$cm.[24] Comparing the third and fourth row one sees that the two point average Z_{wind} differs 10% from the path average value. In all tables values for the quantity K, defined in Eq. (34), and Z_{wind}/τ are given too. The advantage of specifying K is its weak temperature dependence (only broadening of the Fermi-Dirac distribution), while Z_{wind} strongly depends on temperature through ρ. The variation of K turns out to be less than 1% in a temperature range of 1000 K for aluminum, so K can be considered constant and is shown in the sixth column of Table I. The theoretically purest quantity to be extracted from our calculation is Z_{wind}/τ, shown in the last column of this table. The calculation of this quantity requires no model for the resistivity whatsoever. A disadvantage of this quantity is the difficulty in comparing it with experimental quantities.

Very recently Ernst *et al.*[25] presented experimental results for bulk electromigration in aluminum. They found an effective valence varying from -5 at 683 K to -3.3 at 883 K. When we use the combination of the Eqs. (1) and (34),

$$Z^*(T)=Z_{\text{direct}}+\frac{K}{\rho(T)}, \tag{38}$$

in order to analyze these measurements, this leads to values of $K=-45\ \mu\Omega$cm and $Z_{\text{direct}}=+1.4$. The value of K is about 1.5 times larger than the calculated value of $-29\ \mu\Omega$cm (see Table I), which is acceptable. It is interesting that the direct valence is very close to the value of half the chemical valence as predicted by Bosvieux and Friedel.[12]

Sorbello[26] has performed model-pseudopotential calculations for self-electromigration in Al and found a K value of $-112\ \mu\Omega$cm. Although a pseudopotential formulation is considered to be suitable for a nearly free-electron system like aluminum, his value is rather different from our calculated value and the experimental value found by Ernst *et al.*[25] On the other hand his value agrees approximately with values given by Lodding,[27] who refers to measurements by Penney.[28] With respect to these experiments we point out that all available theoretical models for bulk electromigration lead to a temperature dependence of the effective valence according to Eq. (38). The measurements of Penney cannot be fitted by this formula.

An interesting phenomenon is the influence of impurities on the electromigration properties of aluminum. The best-known example is the addition of small amounts of copper, which reduces electromigration induced damage effectively. In the hope that other impurities have a similar but stronger effect on electromigration in aluminum, experimentalists tried palladium and silicon on an *ad hoc* basis, but without success. In order to contribute to a microscopic explanation we investigated the influence of copper, palladium, and silicon impurities that are located in the impurity cluster near a migrating aluminum atom.[29] However, we found[30] that on average the effect is small, although the presence of impurity atoms at particular positions can give rise to a considerable reduction of the wind valence. The presence of a palladium atom induces a reduction of about 10% when averaged over

TABLE I. Results for self-electromigration in Al. A τ value of 69 a.u., based on a resistivity $\rho=8.6\ \mu\Omega$cm at 800 K has been used.

	$Z_{\text{wind}}(sp)$	$Z_{\text{wind}}(pd)$	$Z_{\text{wind}}(df)$	Z_{wind}	$K\ (\mu\Omega\text{cm})$	Z_{wind}/τ
Initial position	0.05	−1.24	−0.12	−1.31	−11.3	−0.019
Saddle point	−0.13	−6.45	0.31	−6.27	−54.0	−0.091
Two point average	−0.04	−2.61	0.13	−3.79	−32.7	−0.055
Path average	0.02	−3.54	0.17	−3.36	−28.9	−0.051

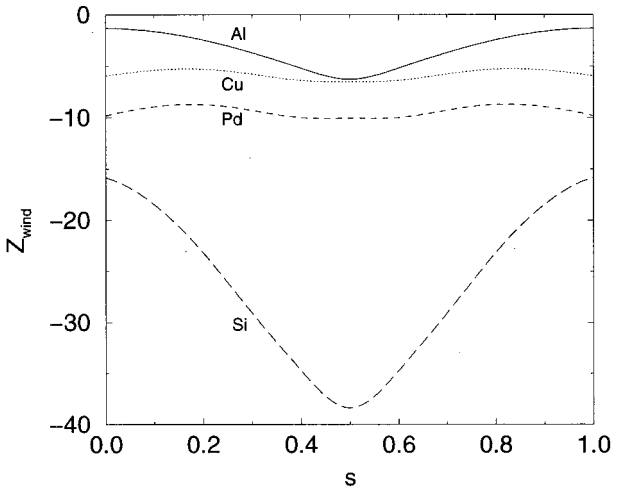

FIG. 3. The position dependent wind valence of copper, palladium, and silicon impurities in Al.

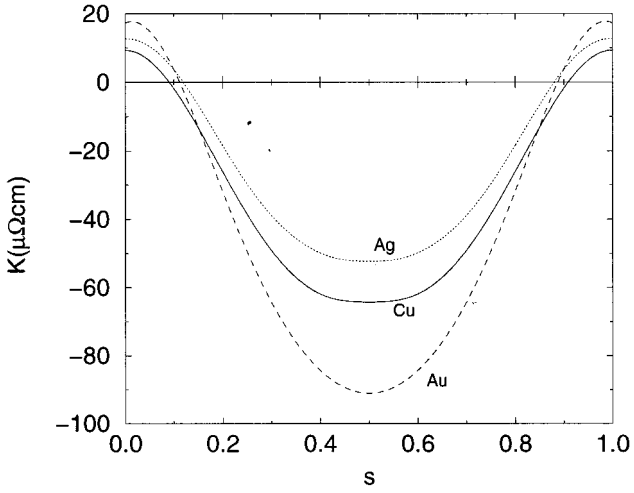

FIG. 4. Variation of K along the path for self-electromigration in Cu, Ag, and Au.

all positions neighboring the migration path (shaded atoms in Fig. 1). The effect of silicon and copper is even smaller.

The presence of impurities changes the number of valence electrons in the system. Within a rigid band model this corresponds to a change of the Fermi energy. A vacancy or a copper atom lowers the Fermi level, while silicon raises ϵ_F. The addition of 1% of copper reduces the average number of valence electrons per atom from 3.0 to 2.98. According to our calculations[30] this reduces the wind valence only by a few percent. The conclusion is that copper atoms do not reduce the wind valence of aluminum atoms directly through electronic effects.

Finally we mention the effect of impurities due to their contribution to the electrical resistivity, which causes a decrease of the wind valence. An addition of 1% of copper induces a resistivity increase of about 10% and the wind valence will be reduced by about 10%.

We conclude that all impurity effects considered above do not induce a dramatic change in the value of the wind valence. Therefore the reduction of the electromigration induced damage cannot be attributed to them.

2. Impurities in aluminum

Besides effects on the electromigration properties of host atoms, impurity atoms can electromigrate themselves. In principle, impurities can migrate in a direction opposite to host atom transport. However, the path dependent wind valences of copper, palladium, and silicon, shown in Fig. 3, all have a negative sign and are larger in magnitude than Z_{wind} of aluminum, which is shown for comparison. This rather accelerates the vacancy transport than slowing it down. The average wind valences of copper, silicon, and palladium are factors of 1.7, 2.8, and 7.8, respectively, larger than Z_{wind} of aluminum. This is in partial contradiction with measurements, quoted by Ho and Kwok[3] in their review article, giving copper a smaller wind valence than host aluminum. We note that the calculated ratios are independent of the model for the calculation of τ, because τ is a host quantity. The fact that the wind valences of the impurities have the same sign is not surprising, because the direction of the force is mainly determined by the direction of the motion of the charge carriers. It is worth noting, that the assumption of a sinusoidal variation of the wind valence along the path does not hold both for copper and palladium, which can be seen clearly in Fig. 3. This means that, in general, the average using only the initial and saddle point position values is not a good measure for the average over the entire path.

B. Electromigration in the noble metals

In this subsection self-electromigration in the noble metals copper, silver, and gold is studied as well as impurity migration in silver.

1. Self-electromigration in copper, silver, and gold

The variation of K along the path for self-electromigration in the noble metals copper (solid line), silver (dotted), and gold (dashed) is shown in Fig. 4. A sign change from positive at the initial site to negative further down the path is observed. This cannot be understood in terms of electron and hole conduction and a free-electron-like model is not able to reproduce such behavior.

The calculated K values listed in Table II cannot be compared with experiment, because as far as a temperature dependence of the effective valence has been measured,[31,32] the results cannot be interpreted in terms of a constant K. But it is interesting to compare them to K values calculated by Gupta[23] and Sorbello.[26] Our values for copper and silver compare very well with the ones of Gupta, while our value for gold is a factor of two smaller. The values of Sorbello are very different from our results, which is not surprising in

TABLE II. Calculated K values for the noble metals compared with results by Gupta (Ref. 23) and Sorbello (Ref. 26).

	Present work	Gupta (Ref. 23)	Sorbello (Ref. 26)
Cu	−33.3	−31.5	−196
Ag	−24.7	−33.1	−171
Au	−42.6	−83.2	−229

TABLE III. Wind and effective valences for the noble metals. The second and third columns contain the calculated wind valence and the measured effective valence, respectively, at the temperature shown in the fourth column. The last column contains the quantity $Z_{\mathrm{wind}}(\mathrm{total})/\tau$ in atomic units.

	Z_{wind}	Z^*	T (K)	Z_{wind}/τ
Cu	−3.5	−4.3 (Ref. 33)	1300	−0.028
Ag	−3.3	−19.9 (Ref. 31)	1150	−0.021
		−5.1 (Ref. 34)		
Au	−3.4	−6.6 (Ref. 32)	1289	−0.037

view of the pseudopotential method he used. However, similar trends are found in our and in Sorbello's calculations: gold shows the largest value of K, while silver shows the smallest. In the calculation of Gupta the K value of copper is the smallest.

In Table III we give calculated Z_{wind} and measured Z^* values[31–34] at a given temperature T, while the last column contains the quantity Z_{wind}/τ. The calculated wind valences are of the same order of magnitude as the experimental effective valences, except for the much larger Z^* of Doan and Brebec for silver.[31] In order to make a detailed comparison between theory and experiment more experimental information is needed.

2. Impurities in silver

This section is devoted to the wind valence of palladium, silver, cadmium, indium, tin, and antimony impurities in silver. The series is part of row 5 in the Periodic System. The calculated wind valence essentially follows the trend of the experimental residual resistivity[24] as is shown in Fig. 5, where both quantities are given as a function of the chemical valence. Both quantities are normalized with respect to the largest values, which occur for antimony. Note that the wind valence of the cadmium impurity is smaller than the one of the host atom.

With the exception of palladium, Doan[35] investigated this series of impurities experimentally and found the effective

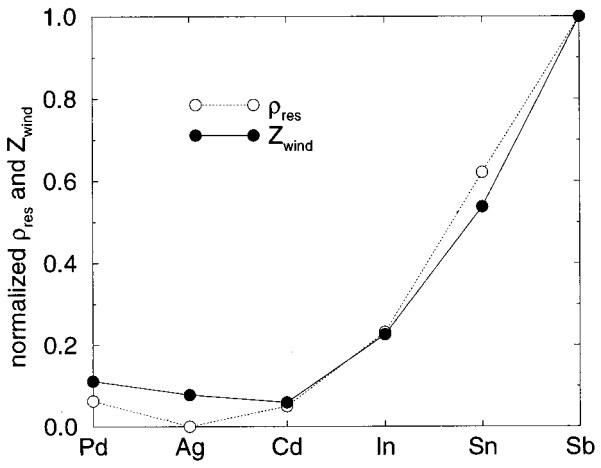

FIG. 5. Measured residual resistivity and calculated wind valence of Pd, Ag, Cd, In, Sn, and Sb impurities in Ag. Both curves are normalized with respect to the Sb data.

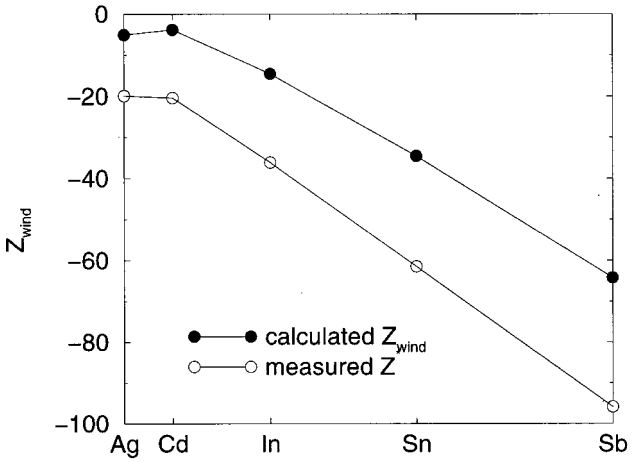

FIG. 6. The solid circles give the calculated wind valence of the atoms Ag, Cd, In, Sn, and Sb, in Ag as a function of $z(z+1)$, where $z=Z_{\mathrm{atom}}-Z_{\mathrm{Ag}}$. The open circles are effective valences, measured by Doan (Ref. 35) at temperatures of approximately 1150 K.

valence to be linear with $z(z+1)$, where $z=Z_{\mathrm{imp}}-Z_{\mathrm{Ag}}$, with Z_{imp} and Z_{Ag} the chemical valence of the impurity and silver atoms, respectively. This dependence is a result of Mott's theory for Born scattering, which leads to a wind valence of an impurity atom proportional to z^2 at its initial position (neglecting backscattering from the vacancy) and to $Z_{\mathrm{imp}}^2=(z+1)^2$ at the saddle point. The calculated Z_{wind} and the measured Z^* at about 1150 K are given as a function of $z(z+1)$ in Fig. 6. Measurements and calculations show a similar trend, but the values do not agree. Neither the measured Z^* nor the calculated Z_{wind} of the silver atom show the $z(z+1)$ dependence.

More information about the trend in the wind valence can be extracted by considering the sp, pd, and df contributions separately. They are plotted in Fig. 7 for the initial and saddle point position, respectively. A transport relaxation time of $\tau=243$ is used, corresponding to a resistivity of $\rho=4.9\ \mu\Omega$cm at 800 K.[24] The pd term turns out to determine the overall behavior. It develops as soon as the p states of the impurity atom are occupied, starting with indium. Note that for the saddle point configuration the sp term van-

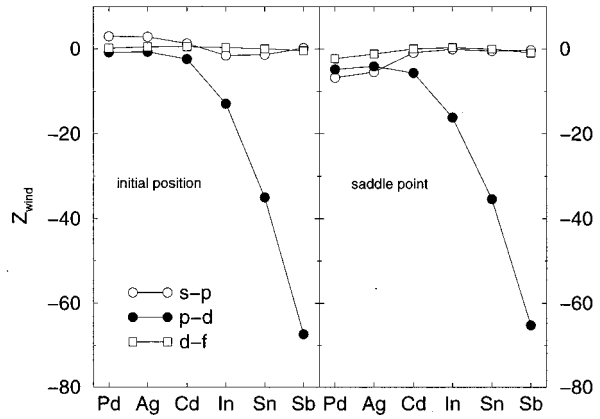

FIG. 7. sp, pd, and df contributions to the wind valence of $4d$ and $5sp$ impurities in Ag at $T=800$ K.

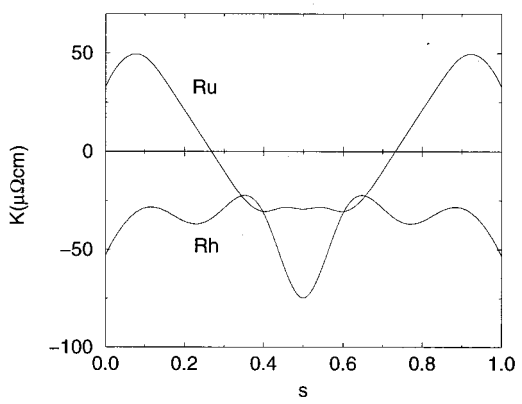

FIG. 8. Variation of K along the migration path for Rh and Ru self-electromigration.

ishes when the $5s$ orbit is completely filled, at cadmium, and leads to a relatively low wind valence of cadmium. A possible origin of it can be the following. In the saddle point configuration the impurity replaces two host atoms. For an impurity atom with filled $5s$ orbitals, two $5s$ electrons are present, just as in the configuration with host atoms in initial and final positions, which is just the host configuration. Such an impurity at the saddle point resembles an unperturbed host state as far as the s electrons are concerned. It may be the case that scattering involving these orbitals is weaker than when just one $5s$ electron is present.

C. Self-electromigration of the 4*d* transition metal

We also applied the theory to the $4d$ transition metals, mainly as a challenge to experimentalists. To our knowledge only electrotransport in zirconium has been measured,[3] showing a small positive effective valence of 0.3. A small positive valence has also been measured for the $5d$ transition metal platinum. Only metals with a close-packed structure are considered in this series of calculations. Metals with the hexagonal close-packed (hcp) structure, namely, yttrium, zirconium, technetium, and ruthenium, are treated as fcc metals.

Remarkable variations of K along the path occur, as shown for rhodium and ruthenium in Fig. 8. One observes minima, maxima, and sign changes. Simple models will fail to describe such features. It should be stressed that the variations occur in spite of the smoothly varying phase shifts, so they are likely to occur due to multiple scattering effects.

The K values averaged over the path are given in Table IV. In our procedure for the construction of the potentials the atomic configuration is important. The electronic configuration of a free atom sometimes differs from that of an atom embedded in a crystal. This is the case for palladium, which has a $4d^9 5s^1$ configuration in the crystal, while the free atom has a $4d^{10} 5s^0$ configuration. The electronic configuration of a host atom in a rhodium crystal lies somewhere between the $4d^8 5s^1$ and $4d^9 5s^0$ configurations. As can be seen from the table the value of K depends only slightly on the configuration used. So the wind valence appears to be only weakly dependent on the precise electronic structure obtained from non-self-consistent potentials. Although it remains interesting to investigate the influence of self-consistency we do not expect large effects for a metal like rhodium. Looking along the series in Table IV no clear trend is observed in the K values.

TABLE IV. The calculated K and Z_{wind} at a temperature T for the $4d$ transition metals. The transport relaxation time τ at that T is given in atomic units.

	K ($\mu\Omega$cm)	T (K)	Z_{wind}	τ (a.u.)
Y	93.2	1700	0.4	25.4
Zr	−52.1	1700	−0.4	13.7
Tc	34.8	1700	0.5	12.4
Ru	7.0	1500	0.2	10.6
Rh($4d^8 5s^1$)	−36.9	1700	−1.0	13.0
Rh($4d^9 5s^0$)	−38.3	1700	−1.0	12.7
Pd	−58.6	1700	−1.3	50.4

Also shown are the wind valences at a certain (high) temperature and the transport relaxation time τ used to calculate it. The effective valence of zirconium, which was measured to be $+0.3$, is not in contradiction with the value of -0.4 for the wind valence However, it should be mentioned that the experiments were done at high temperatures in the α phase of zirconium. The wind valence for this phase, having the bcc structure, will be calculated in the near future. As can be seen in the table, the wind valence in the $4d$ transition metals turns out to be small. On the other hand, the chemical valence can be rather large and therefore the effective valence is dominated by the direct valence and varies only slightly with temperature. Hence, these transition metals are suitable for the experimental determination of the direct valence, which has been the subject of a long-lasting controversy.[4]

V. CONCLUSIONS

We have improved a Green's function method for the calculation of the electronic structure in dilute alloys. The formalism has been applied to the calculation of the wind force in the case of substitutional electromigration. We have focused on fcc and hcp metals with the hcp metals treated in the fcc structure.

The calculated wind valence for self-electromigration in aluminum is in acceptable agreement with recent measurements of Ernst *et al.*[25] We have also investigated the effect of the presence of impurities on the wind valence of aluminum. Neither the presence of an impurity atom near the jump path nor the impurity induced increase of the total resistivity of aluminum induces a dramatic change of the wind valence. So, changes in the electronic structure due to the presence of an impurity are not the reason for a reduction of Z_{wind}.

The wind valence for self-electromigration in the noble metals shows a sign change along the path. Such a behavior cannot be reproduced by simple models. Path averaged values show qualitative agreement with experiment.

Calculated wind valences of cadmium, indium, tin, and antimony in silver roughly follow the measured residual resistivity and are approximately linear with $z(z+1)$, where z is the difference in chemical valence between the impurity and the silver. Such a trend was predicted within Mott's theory for Born scattering in metals and has been observed

experimentally, although the precise values of the wind valence do not agree very well.

Finally the wind valences for self-electromigration in the $4d$ transition metals show a large variation in size and sign. The average values often are small due to cancellation of the wind valence along the migration path. The effective valence therefore is dominated by the direct valence and will depend on temperature only weakly. Hence, measurements on these metals are suitable to decide which model for the direct force is the correct one.

ACKNOWLEDGMENTS

This work was sponsored by the Stichting Nationale Computerfaciliteiten (National Computing Facilities Foundation, NCF) for the use of supercomputer facilities, with financial support from the Nederlandse Organisatie voor Wetenschappelijk Onderzoek (Netherlands Organization for Scientific Research, NWO).

APPENDIX A

First Eq. (14) will be derived from Eq. (9). In Eq. (14), written in the position representation, one substitutes the local Schrödinger equation

$$v^p(\mathbf{x})\Psi_k(\mathbf{x}+\mathbf{R}_p)=(\nabla^2+E)\Psi_k(\mathbf{x}+\mathbf{R}_p). \tag{A1}$$

Then one applies Green's theorem and uses the equation for the void Green's function

$$(\nabla^2+E)G^{\text{void}}(\mathbf{r},\mathbf{r}')=\delta(\mathbf{r}-\mathbf{r}'), \tag{A2}$$

as it holds inside the void region. By that the void wave function can be written as a sum of spherical surface integrals,

$$\begin{aligned}\Psi_k^{\text{void}}(\mathbf{x}+\mathbf{R}_p)=\sum_{p'}\int_{S_{p'}}d\mathbf{S}_{p'}[\nabla' G^{\text{void}}(\mathbf{x}+\mathbf{R}_p,\mathbf{x}'+\mathbf{R}_{p'})]\\ \times\Psi_k(\mathbf{x}'+\mathbf{R}_{p'})-G^{\text{void}}(\mathbf{x}+\mathbf{R}_p,\mathbf{x}'+\mathbf{R}_{p'})\\ \times\nabla'\Psi_k(\mathbf{x}'+\mathbf{R}_{p'}).\end{aligned} \tag{A3}$$

Using Eq. (11) for the void Green's function and the form of the local basis functions at the boundaries of the cell in Eq. (5), Eq. (A3) can be elaborated for small x. This leads to the expression (14) for the void wave function coefficients of Eq. (10) in terms of the alloy wave function coefficients of Eq. (4).

Now we want to illustrate the derivation of Eq. (16), the relation between c_{kpL}^{void} and c_{kjL}^{void}. This can be found by working out the void wave function for a position $\mathbf{r}=\mathbf{x}+\mathbf{R}_j=\mathbf{x}_p+\mathbf{R}_p$, which is a position in the alloy cell labeled by p and in the host cell labeled by j,

$$\Psi_k^{\text{void}}(\mathbf{r})=\sum_L c_{kpL}^{\text{void}}j_L(\mathbf{x}_p)=\sum_L c_{kjL}^{\text{void}}j_L(\mathbf{x}). \tag{A4}$$

The two Bessel functions centered at different positions are related by

$$j_L(\mathbf{x})=j_L(\mathbf{x}_p+\mathbf{R}_{pj})=\sum_{L'} j_{L'}(\mathbf{x}_p)J_{L'L}^{pj}, \tag{A5}$$

in which the matrix J^{pj} is given by

$$J_{LL'}^{pj}=4\pi i^{l-l'}\sum_{L''} i^{l''}C_{LL'L''}j_{L''}(\mathbf{R}_{pj}). \tag{A6}$$

Substitution of this equation in Eq. (A4) automatically leads to Eq. (16).

APPENDIX B

It will be shown how the infinite angular momentum summation in Eq. (17) can be carried out analytically, leading to Eq. (18). In addition Eq. (25) is generalized to Eq. (31), valid for arbitrary position labels.

First a relation between $\mathcal{G}^{\text{void},pp'}$, present in the left hand side of Eq. (17), and $\mathcal{G}^{\text{void},jj'}$ will be derived. To that end the void Green's function $G^{\text{void}}(\mathbf{r},\mathbf{r}')$ for the positions $\mathbf{r}=\mathbf{x}+\mathbf{R}_j=\mathbf{x}_p+\mathbf{R}_p$ and $\mathbf{r}'=\mathbf{x}'+\mathbf{R}_{j'}=\mathbf{x}'_{p'}+\mathbf{R}_{p'}$, see Eq. (11), is rewritten using the free-space Green's function (12). It follows that

$$\begin{aligned}G^{\text{void}}(\mathbf{r},\mathbf{r}')&=G^0(\mathbf{r},\mathbf{r}')+\sum_{LL'} j_L(\mathbf{x}_p)(\mathcal{G}_{LL'}^{\text{void},pp'}-B_{LL'}^{pp'})j_L(\mathbf{x}'_{p'})\\ &=G^0(\mathbf{r},\mathbf{r}')+\sum_{LL'} j_L(\mathbf{x})(\mathcal{G}_{LL'}^{\text{void},jj'}-B_{LL'}^{jj'})j_L(\mathbf{x}').\end{aligned} \tag{B1}$$

Applying Eq. (B1) and using Eq. (A5) straightforwardly leads to

$$\mathcal{G}^{\text{void},pp'}=B^{pp'}+J^{pj}(\mathcal{G}^{\text{void},jj'}-B^{jj'})J^{j'p'}. \tag{B2}$$

Now the right hand side of Eq. (17) is rewritten using the KKR equation (20) and Eq. (21)

$$\begin{aligned}\sum_{j'} J^{pj}(1-\mathcal{G}^{\text{void}}t^h)^{jj'}c_{kj'}^{\text{host}}\\ =J^{pj}b(\mathbf{k})t^h c_{kj}^{\text{host}}-\sum_{j'} J^{pj}\mathcal{G}^{\text{void},jj'}t^h c_{kj'}^{\text{host}}.\end{aligned} \tag{B3}$$

The first term on the right hand side of this equation can be evaluated using the expansion

$$B^{pj'}=J^{pj}B^{jj'},\quad (R_{pj}<R_{jj'}), \tag{B4}$$

which can be derived from an expansion for the Hankel function similar to Eq. (A5) for the Bessel function. From the definition of $b(\mathbf{k})\equiv b(\mathbf{k},0)$, see Eq. (19), it follows that

$$J^{pj}b(\mathbf{k})=b(\mathbf{k},\mathbf{R}_p)e^{i\mathbf{k}\cdot\mathbf{R}_{pJ}}-B^{pj}. \tag{B5}$$

Substituting this equation in Eq. (B3) the first term on the right hand side of Eq. (18) appears, and one has to deal further with the terms,

$$-\sum_{j'}(B^{pj'}\delta_{jj'}+J^{pj}\mathcal{G}^{\text{void},jj'})t^h c_{kj'}^{\text{host}}. \tag{B6}$$

The sum of matrices $B^{pj'}\delta_{jj'}+J^{pj}\mathcal{G}^{\text{void},jj'}$ can be written as $B^{pj'}+J^{pj}(\mathcal{G}^{\text{void},jj'}-B^{jj'})$. The latter sum is equal to

$\mathcal{G}^{\text{void},pj'}$, given by Eq. (B2) with p' replaced by a host label j'. By this Eq. (B3) obtains the form of Eq. (18).

Now we turn to the derivation of Eq. (31). Substitution of Eq. (25) in Eq. (B2) yields

$$\mathcal{G}^{\text{void},pp'} = B^{pp'} + J^{pj}(\mathcal{G}^{jj'} - B^{jj'})J^{j'p'} - \sum_{j_1 j_2} J^{pj}\mathcal{G}^{jj_1}(t^{h^{-1}} + \mathcal{G})^{-1}_{j_1 j_2}\mathcal{G}^{j_2 j'}J^{j'p'}. \quad \text{(B7)}$$

Regarding Eq. (30) for $\mathcal{G}^{jj'}$ one has to apply Eq. (B5) for a further reduction. Using the straightforward generalization of the host Green's function matrix (30), defined by

$$\mathcal{G}^{pp'} \equiv \frac{1}{\Omega_{\text{BZ}}}\int_{\text{BZ}} d^3k[\,b(\mathbf{k},\mathbf{R}_{pp'}) + b(\mathbf{k},\mathbf{R}_p)M^{-1}(\mathbf{k})b^T(-\mathbf{k},\mathbf{R}_{p'})]e^{i\mathbf{k}\cdot\mathbf{R}_{pp'}}, \quad \text{(B8)}$$

the following relations can be derived:

$$J^{pj}(\mathcal{G}^{jj'} - B^{jj'})J^{j'p'} = \mathcal{G}^{pp'} - B^{pp'} - \mathcal{G}^{pj'}t^h B^{j'p'} - B^{pj}t^h\mathcal{G}^{jp'} + B^{pj}t^h(t^{h^{-1}} + \mathcal{G})^{jj'}t^h B^{j'p'}, \quad \text{(B9a)}$$

$$J^{pj}\mathcal{G}^{jj_1} = \mathcal{G}^{pj_1} - B^{pj}t^h(t^{h^{-1}} + \mathcal{G})^{jj_1}, \quad \text{(B9b)}$$

$$\mathcal{G}^{j_2 j'}J^{j'p'} = \mathcal{G}^{j_2 p'} - (t^{h^{-1}} + \mathcal{G})^{j_2 j'}t^h B^{j'p'}. \quad \text{(B9c)}$$

Substituting these equations in Eq. (B7) gives the desired form (31),

$$\mathcal{G}^{\text{void},pp'} = \mathcal{G}^{pp'} - \sum_{j_1 j_2}\mathcal{G}^{pj_1}(t^{h^{-1}} + \mathcal{G})^{-1}_{j_1 j_2}\mathcal{G}^{j_2 p'}. \quad \text{(B10)}$$

[1] A. Coehn and W. Specht, Z. Phys. **62**, 1 (1930).
[2] R. S. Sorbello, A. Lodder, and S. J. Hoving, Phys. Rev. B **25**, 6178 (1982).
[3] P. S. Ho and T. Kwok, Rep. Prog. Phys. **52**, 301 (1989).
[4] A. Lodder, Solid State Commun. **79**, 143 (1991).
[5] J. Korringa, Physica (The Hague) **13**, 392 (1947).
[6] W. Kohn and N. Rostoker, Phys. Rev. **94**, 1111 (1954).
[7] A. Lodder, J. Phys. F **6**, 1885 (1976).
[8] A. Lodder, J. Phys. F **14**, 2943 (1984).
[9] J. van Ek, J. P. Dekker, and A. Lodder, Phys. Rev. B **52**, 8794 (1995).
[10] P. M. Oppeneer and A. Lodder, J. Phys. F **17**, 1885 (1987).
[11] J. van Ek and A. Lodder, J. Phys.: Condens. Matter **3**, 7307 (1991).
[12] C. Bosvieux and J. Friedel, J. Phys. Chem. Solids **23**, 123 (1962).
[13] R. K. Nesbet, Phys. Rev. B **41**, 4948 (1990).
[14] J. M. Ziman, in *Principles of the Theory of Solids*, edited by J. M. Ziman (Cambridge University Press, Cambridge, 1972).
[15] V. B. Fiks, Fiz. Tverd. Tela. **1**, 16 (1959) (Leningrad) [Sov. Phys. Solid State **1**, 14 (1959)].
[16] H. B. Huntington and A. R. Grone, J. Phys. Chem. Solids **20**, 76 (1961).
[17] P. Kumar and R. S. Sorbello, Thin Solid Films **25**, 25 (1975).
[18] J. van Ek and A. Lodder, J. Phys.: Condens. Matter **3**, 7331 (1991).
[19] J. Molenaar, A. Lodder, and P. T. Coleridge, J. Phys. F **13**, 839 (1983).
[20] P. M. Oppeneer and A. Lodder, J. Phys. F **17**, 1901 (1987).
[21] A. Lodder and P. J. Braspenning, Phys. Rev. B **49**, 10 215 (1994).
[22] R. H. Lasseter and P. Soven, Phys. Rev. B **8**, 2476 (1973).
[23] R. P. Gupta, Phys. Rev. B **25**, 5188 (1982).
[24] J. Bass, in *Metals: Electronic Transport Phenomena*, edited by K.-H. Hellwege and J. L. Olsen, Landolt-Börnstein, New Series, Group III, Vol. 15, pt. a (Springer-Verlag, Berlin, 1982).
[25] B. Ernst, G. Frohberg, and H. Wever, Def. Diff. Forum **143-147**, 1649 (1997).
[26] R. S. Sorbello, J. Phys. Chem. Solids **34**, 937 (1973).
[27] A. Lodding, J. Phys. Chem. Solids **26**, 143 (1964).
[28] R. V. Penney, J. Phys. Chem. Solids **25**, 335 (1964).
[29] A. Lodder and J. P. Dekker, in *Proceedings of the First International Alloy Conference, Athens, 1996*, edited by A. Gonis, A. Meike, and P. E. A. Turchi (Plenum, New York, 1997).
[30] J. P. Dekker and A. Lodder, Def. Diff. Forum **143-147**, 1645 (1997).
[31] N. V. Doan and G. Brebec, J. Phys. Chem. Solids **31**, 475 (1970).
[32] H. M. Gilder and D. Lazarus, Phys. Rev. **145**, 507 (1966).
[33] G. A. Sullivan, J. Phys. Chem. Solids **28**, 347 (1967).
[34] H. R. Patil and H. B. Huntington, J. Phys. Chem. Solids **31**, 463 (1970).
[35] N. V. Doan, J. Phys. Chem. Solids **31**, 2079 (1970).